Physics Open 1 (2019) 100001

Contents lists available at ScienceDirect

Physics Open

journal homepage: www.journals.elsevier.com/physics-open

Manifestations of chaos in relativistic quantum systems - A study based on out-of-time-order correlator

Chen-Di Han [a], Hong-Ya Xu [a], Liang Huang [b], Ying-Cheng Lai [a,c,*]

[a] School of Electrical, Computer and Energy Engineering, Arizona State University, Tempe, AZ, 85287, USA
[b] School of Physical Science and Technology, Key Laboratory for Magnetism and Magnetic Materials of MOE, Lanzhou University, Lanzhou, Gansu, 730000, China
[c] Department of Physics, Arizona State University, Tempe, AZ, 85287, USA

ARTICLE INFO

Handling editor: Matteo Paris

Keywords:
Relativistic quantum chaos
OTOC
Dirac equation
Schrödinger equation
Chaotic billiards
Level spacing statistics

ABSTRACT

Previous work in the field of relativistic quantum chaos has revealed initial evidence that the manifestations of classical chaos in relativistic quantum systems tend to be weakened as compared with those in nonrelativistic quantum systems. To place this finding on a firmer ground, we investigate the relativistic quantum fingerprints of classical chaos using the out-of-time-order correlator (OTOC). OTOC has recently been applied to a number of fields in physics and it holds special promises for the field of quantum chaos, but existing work focused exclusively on nonrelativistic quantum systems. Calculating and analyzing OTOC for relativistic quantum billiard systems described by the massless Dirac equation, we find that the signatures of classical chaos are indeed characteristically less pronounced in relativistic than in nonrelativistic quantum systems. The finding is substantiated by studying four different aspects of OTOC. Firstly, in the energy eigenspace, in the short time regime there is a complete lack of any signature of chaos associated with the evolution of OTOC in the Dirac billiard due to the relativistic quantum phenomenon of Zitterbewegung, in contrast to nonrelativistic quantum billiard systems where chaos leaves behind a quite distinct signature. Secondly, weakening of the relativistic quantum manifestations of classical chaos occurs in the long time regime as well. Thirdly, evolution of the wave packet based OTOC also reveals that the fingerprints of chaos are much less pronounced in the Dirac billiard systems as compared with the Schrödinger billiards. Fourthly, the level spacing statistics of the OTOC operators in systems with classically integrable and chaotic dynamics, which are characteristically distinct in the Schrödinger billiards, bear a strong similarity in the Dirac billiards, indicating again the dwindling effects of chaos. The OTOC based results suggest that the impacts of classical chaos are generally weaker in relativistic than in nonrelativistic quantum systems, a fundamental issue that warrants further investigation.

1. Introduction

When chaos meets with (non relativistic) quantum mechanics, a set of signatures is left behind [1–3]. For example, in a closed chaotic Hamiltonian system, the probability for an infinitesimal separation between two neighboring energy levels diminishes [4–6], in contrast to an integrable system where this probability is most pronounced. In a closed chaotic billiard system, the eigen-wavefunctions can concentrate about the unstable periodic orbits that are the fundamental building blocks of classical chaos - the phenomenon of quantum scarring [7,8]. In electronic transport through a quantum dot structure whose geometry generates chaos in the classical limit, the fluctuations in the quantum transmission or conductance can be greatly smoothed out in comparison with the situation where the dot geometry produces classically integrable dynamics [9]. Classical chaos can also lead to localization of the wavefunctions [10]. The study of the manifestations of classical chaos in the corresponding (nonrelativistic) quantum system constitutes the field of quantum chaos [1–3], which has been active for four decades.

Recently, *relativistic quantum chaos* (RQC) [11,12] has emerged as a field to study the signatures of classical chaos in relativistic quantum systems. The main motivation for RQC came from the tremendous interest in and development of two-dimensional (2D) Dirac materials [13,14] such as graphene [15–21] and topological insulators [22]. The energy bands of these materials typically contain a Dirac cone structure, stipulating a linear energy-momentum dispersion relation near a Dirac point. In this energy regime, the quasiparticles of the materials are

* Corresponding author. School of Electrical, Computer and Energy Engineering, Arizona State University, Tempe, AZ, 85287, USA.
E-mail address: Ying-Cheng.Lai@asu.edu (Y.-C. Lai).

https://doi.org/10.1016/j.physo.2019.100001
Received 15 July 2019; Accepted 30 July 2019
Available online 30 August 2019

pseudospin-1/2 fermions and are described by the massless Dirac equation for a two-component pseudospinor. Studies of RQC have revealed a relatively stronger suppression of chaos in relativistic quantum than in nonrelativistic quantum systems. For example, in a study [23] on electronic transport through quantum dots that exhibit different types of classical scattering dynamics (e.g., integrable or chaotic), in the Schrödinger system, classical chaos can dramatically smooth out the sharp fluctuations associated with resonances in quantum transmission or conductance that would be present if the classical dynamics were integrable, a phenomenon that can be exploited for chaos based modulation or control of quantum transport characteristics [24,25]. However, in a relativistic quantum graphene dot, sharp resonances are still present in the transmission even when the corresponding classical dynamics become fully chaotic [23]. Another example is persistent currents [26–29], permanent currents in the absence of any external power source, in a ring domain with a central magnetic flux that breaks the time reversal symmetry. The currents have been observed in a variety of nonrelativistic quantum material systems [30–37]. Random impurities in metallic or semiconductor systems tend to diminish the persistent currents [38–45], where they decay exponentially to zero as the disorder strength is increased. In fact, in a Schrödinger ring system, boundary deformations leading to classical chaos typically destroy persistent currents [46,47] as effectively as random disorder. However, in graphene or other Dirac materials, persistent currents were found to be robust [48–60]. A theoretical study demonstrated that, in Dirac ring systems, even when there are substantial boundary deformations leading to fully developed chaos in the classical limit, persistent currents of comparable magnitude with that in the integrable ring system can arise (henceforth the term "super persistent currents") [46,47]. From the point of view of the quantum signatures of classical chaos, it can be understood that the signatures of chaos are less pronounced in the Dirac ring system as compared with the corresponding Schrödinger ring.

The purpose of this paper is to establish the weakening of chaos in relativistic quantum systems on a firm ground based on a comprehensive analysis of the out-of-time-order correlator (OTOC). Historically, OTOC was proposed in the field of superconductivity [61]. In basic quantum mechanics, OTOC measures the degree of commutation between two operators, which can be used to characterize diverse physical phenomena such as operator spreading [62,63], growth in quantum entanglement [64,65], and nuclear magnetic resonances [66]. Recently, the study of OTOC has attracted a great deal of attention due to its relevance to a large number of fields in physics. For example, OTOC has been employed to search for the quantum butterfly effect in many body systems such as those described by the Ising model [67,68] and the Sachdev-Ye-Kitaev (SYK) model [69,70]. In high energy physics, OTOC has been exploited to establish the correspondence between conformal field theory (CFT) and holography [71]. More recently, OTOC has been introduced into the field of quantum chaos [64–76]. To our knowledge, all existing studies on OTOC to uncover and characterize the signatures of classical chaos were for nonrelativistic quantum systems described by the Schrödinger equation.

In this paper, we consider 2D classically integrable and chaotic billiards, and calculate the OTOC defined in the context of Dirac equation. For comparison, we also do the calculations for the corresponding Schrödinger system. For convenience, in this paper we use the terms "nonrelativistic quantum" and "Schrödinger" interchangeably, as well as the terms "relativistic quantum" and "Dirac." In previous studies of OTOC in nonrelativistic quantum chaotic systems [74–76], an important time scale was defined: the Ehrenfest or the scrambling time [72] within which the dynamics of the system are essentially classical and any quantum interference effect can be ignored. We find it necessary to introduce another time scale: the revival time t_R, to characterize the quantum oscillatory motion [77], where the relativistic quantum behavior of the system is distinct before and after this time [78]. We systematically study OTOC in various situations (classically integrable versus chaotic dynamics, relativistic versus nonrelativistic quantum mechanics) from four different angles that mutually support each other: short and long time evolution of OTOC in the energy eigenspace, wave packet based evolution of OTOC, and level spacing statistics of the OTOC operator.

The main findings are as follows. Firstly, in the short time regime defined by $t < t_R$, the microcanonical thermal averaged value of OTOC is strongly indicative of Zitterbewegung motion - relativistic quantum oscillations with no counterpart in Schrödinger systems. A striking phenomenon is that the oscillations are independent of the nature of the classical dynamics: their characteristics are nearly identical for the integrable and chaotic systems. This means that, in short time, fingerprints of classical chaos are completely lost in the relativistic quantum realm, in stark contrast to the behavior in nonrelativistic quantum systems. Secondly, in the long time regime ($t > t_R$), OTOC exhibits oscillations that can be related to wave-packet revival. The evolutionary behaviors are quite distinct in Schrödinger billiards with classically integrable and chaotic dynamics, but they again are similar for the Dirac billiards. In fact, for the latter, some signatures of classical chaos appear but only in the asymptotic time regime. Thirdly, we exploit semiclassical propagation [79] through wave packet revival [80] by calculating the time evolution of the wave packet based OTOC, which reveals essentially the same phenomenon. Finally, we carry out a spectral analysis of the OTOC operator and find that, in Schrödinger systems with classical integrable or chaotic dynamics, the eigenvalue spacing distribution exhibits characteristics of Poisson random matrices or those of Gaussian Orthogonal Ensemble (GOE), respectively, which agree completely with the energy level spacing statistics [4]. A surprising result is that, for the Dirac billiards, the level spacing statistics for integrable and chaotic dynamics bear a marked similarity. The findings from the four perspectives of OTOC lead to the conclusion that the effects of classical chaos are generally less pronounced in relativistic than in nonrelativistic quantum systems.

2. OTOC in relation to quantum chaos and its calculation in relativistic quantum systems

2.1. Quantum chaos and OTOC

A long-standing conundrum in the field of quantum chaos concerns the meaning of "chaos." In classical physics, a necessary condition for chaos to arise is that the underlying system be nonlinear, and the hallmark of chaos is a sensitive dependence on initial conditions that gives rise to an exponential growth of a random infinitesimal vector in phase space, where the rate of growth defines the Lyapunov exponent. In quantum mechanics, however, the fundamental Schrödinger or Dirac equation is linear, so an exponential sensitivity to initial conditions or equivalently, a positive Lyapunov exponent, cannot be expected. There should then be no actual chaos in quantum systems (Sir Michael Berry stated [81] in 1989 that "*There is no quantum chaos, in the sense of exponential sensitivity to initial conditions, but there are several novel quantum phenomena which reflect the presence of classical chaos. The study of these phenomena is quantum chaology*.") Nonetheless, in the development of the field, the term "quantum chaos" has prevailed and has been widely adopted [2,3]. In spite of a quantum system's being fundamentally linear, which excludes chaos, the issue of whether there is exponential sensitivity in quantum systems has been a subject of active debate [82–86] and pursuit [87–89].

Exploiting the general property of OTOC that it measures the separation in time of a commutator of quantum mechanical operators, it has been shown recently that, for a chaotic system in the semiclassical limit $\hbar \to 0$, OTOC exhibits an exponential growth behavior with the rate related to the Lyapunov exponent [72,73]. Explicit calculations of OTOC for the circular (integrable) and stadium (chaotic) billiards were subsequently carried out [74,75] with the finding that OTOC is not recursive (in contrast to the case of, e.g., a one-dimensional harmonic oscillator) but tends to constant values. However, for the chaotic stadium billiard,

OTOC does not exhibit any exponential growth behavior. A driven chaotic system, the kicked rotor, was also studied [76], revealing an exponential growth behavior of OTOC. However, it was found that the exponential rate is not exactly the Lyapunov exponent because of the different order in taking the phase space average and logarithm. In particular, to calculate the OTOC growth rate based on the classical-quantum correspondence, one takes the phase space average of the divergence rate of classical trajectories and then takes the logarithm, while for the Lyapunov exponent, the order of the two operations is reversed, i.e., it is the phase space average of the logarithm of the divergence. Some recent findings [72,76] are consistent with the early result of Robbins and Berry [90] on the discordance between quantum and classical correlation moments for chaotic systems. The current understanding is that a chaotic system in the quantum regime may or may not exhibit an exponential growth behavior in OTOC but, if it does, the exponential growth rate is not the same as the Lyapunov exponent in the corresponding classical system. Nevertheless, studies so far have suggested strongly that OTOC can be a promising theoretical or even experimental tool [64–76] for the field of quantum chaos.

2.2. Calculation of OTOC in relativistic quantum systems

An OTOC is generally defined as

$$\widehat{C}^{\alpha} = (-i)^{\alpha}\langle[\widehat{W}(t), \widehat{V}(0)]^{\alpha}\rangle, \tag{1}$$

where $\widehat{W}$ and $\widehat{V}$ are two Hermitian operators in the Heisenberg picture: $\widehat{W}(t) = \exp(-i\widehat{H}t/\hbar)\widehat{W}\exp(i\widehat{H}t/\hbar)$. The phase factor $(-i)^{\alpha}$ is chosen to ensure that the OTOC is Hermitian and has positive eigenvalues for different values of α. A common choice of α is $\alpha = 2$. In this case, the square of the commutation between the operators $\widehat{W}$ and $\widehat{V}$ at two different instants of time generates the out-of-time order component [91]:

$$\tilde{C} = \widehat{W}(t)\widehat{V}(0)\widehat{W}(t)\widehat{V}(0) + \widehat{V}(0)\widehat{W}(t)\widehat{V}(0)\widehat{W}(t).$$

For the case where $\widehat{W}$ and $\widehat{V}$ are the position and momentum operators: $\widehat{W} = \hat{x}$ and $\widehat{V} = \hat{p}$, in the classical limit $\hbar \to 0$, the OTOC can be related to the Lyapunov exponent associated with the corresponding classical dynamics [73].

The subject of our study is relativistic quantum billiard systems with the Dirac Hamiltonian given by

$$\widehat{H} = v_F\hat{\boldsymbol{\sigma}}\cdot\hat{\boldsymbol{p}} + \hat{\sigma}_z V(\mathbf{r}), \tag{2}$$

where $\hat{\boldsymbol{\sigma}}$ and $\hat{\sigma}_z$ are Pauli matrices, $V(\mathbf{r})$ is a potential field that defines the billiard shape: $V(\mathbf{r}) = 0$ inside the billiard and $V(\mathbf{r}) = \infty$ outside, and v_F is the Fermi velocity of the quasiparticles. The billiard systems are one of the paradigms in the traditional field of nonrelativistic quantum chaos [1–3]. For a billiard system, the nature of the classical dynamics is determined completely by the geometric shape of the boundary. For example, for a circular billiard, the classical dynamics are integrable. In the corresponding quantum system, nonrelativistic or relativistic, the statistical distribution of the energy level spacing is Poisson [4,6], as shown by the blue (Schrödinger) and red (Dirac) curves in Fig. 1(a). If the shape of the billiard is deformed from that of a perfect circle, the classical dynamics are generally nonintegrable with the occurrence of chaos. One of the often studied billiard systems whose classical dynamics are fully chaotic is one with the shape of Africa - the African billiard [6], as shown in the inset of Fig. 1(b). For this system, in the nonrelativistic quantum world with a time reversal symmetry, the energy level spacing distribution follows that of GOE [4], as shown by the blue curve in Fig. 1(b). However, for a massless particle described by the Dirac equation, e.g., a neutrino, the infinite mass confinement breaks the time reversal symmetry, leading to level spacing statistics characteristic of those of Gaussian Unitary Ensemble (GUE) random matrices [6], as shown by the red curve in Fig. 1(b). (For a thorough discussion of the statistics of the energy level spacing for Schrödinger, Dirac, and graphene billiards with classical integrable or chaotic dynamics, see Ref. [12].)

For the two types of billiard systems, we calculate OTOC for both the Schrödinger and Dirac equations. A difficulty with the Dirac equation is that, for the momentum operator $\hat{p}$, the definition of OTOC in Eq. (1) typically leads to divergence (Appendix A). To overcome this difficulty, we take advantage of the feature of spin-momentum coupling in relativistic quantum mechanics, which is absent in the nonrelativistic quantum counterpart. Especially, we choose [68] $\widehat{W} = \widehat{V} = \hat{\sigma}_x$, which corresponds to the current operator $\hat{\sigma}_x = \partial\widehat{H}/\partial\hat{p}_x$ in Dirac systems. For a meaningful comparison, for the nonrelativistic quantum system we use $\widehat{W} = \widehat{V} = \hat{p}_x$. In the semiclassical limit, the choice of the operators $\widehat{W}$ and $\widehat{V}$ is directly related to the evolution of the quantity $[\Delta p_x(t)/\Delta x(0)]^2$, which measures how Δp_x evolves with time for any given initial amount of Δx, a feature that can be studied in classical phase space as well.

For numerical calculation of OTOC in Dirac systems, we use the infinite mass boundary condition [6] and the normalized unit convention $\hbar = 2m = v_F = 1$. For the circular integrable billiard, both the Schrödinger and Dirac equations can be solved analytically. For the chaotic African billiard, we use the method of conformal mapping originally proposed by Robnik for nonrelativistic quantum billiards [92] and later on generalized to relativistic quantum billiards [93] to solve the Schrödinger and Dirac equations in the domain, respectively. Advantages of the conformal mapping method include computational efficiency and extremely high accuracy. For the integrable billiard, we use 10^4~10^5 eigenstates. Because of the need to ensure computational feasibility, for the chaotic billiard we choose 10^3~10^4 eigenstates.

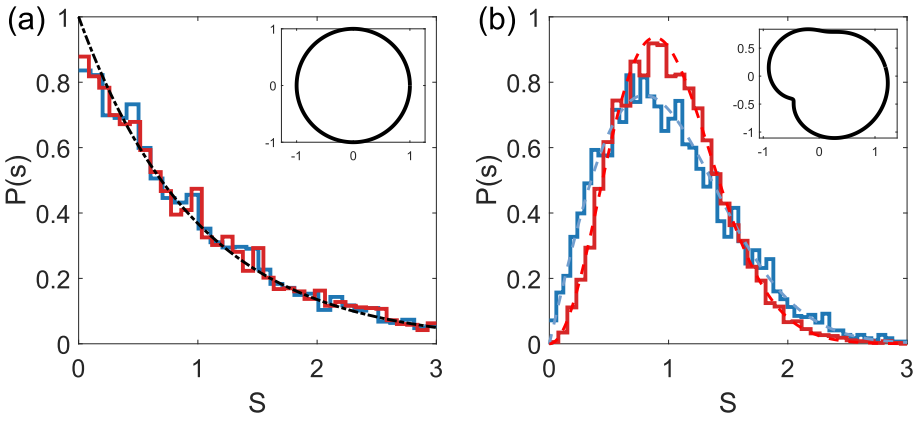

Fig. 1. *Representative billiard systems used in our OTOC study and the statistical distributions of energy level spacing.* (a) A circular billiard with classically integrable dynamics (inset). The energy level spacing distributions are Poisson (black dashed curve) in both the Schrödinger (blue zigzagged curve) and Dirac (red zigzagged curve) quantum worlds. (b) A billiard with the shape of Africa (inset; the African billiard) that exhibits fully developed chaos in the classical limit. The distribution of the energy level spacing is GOE (blue zigzagged curve) for the Schrödinger system and GUE (red zigzagged curve) for the Dirac counterpart.

3. Result 1: evolution of OTOC in short time regime

The initial growth of OTOC in short time has been a focus of previous studies [64–76], due to the possible correspondence to the growth of a small tangent vector in classical phase space as quantified by the Lyapunov exponent. In particular, for a classically chaotic system, an infinitesimal distance between two nearby points tends to grow exponentially with time at the rate determined by the largest Lyapunov exponent. (For convenience, in this paper we refer to the largest Lyapunov exponent simply as the Lyapunov exponent.) The initial growth of OTOC, if it is exponential, would thus be indicative of classical chaos, as speculated in the earlier work [72,73]. However, no exponential growth has been found for the chaotic billiard systems [74,75]. For our relativistic quantum billiard systems, no initial exponential growth in OTOC has been found in numerical computations. For the short time behavior of OTOC, we thus focus on detecting any possible difference between its time evolution in systems with integrable and chaotic dynamics.

In general, we find that the relativistic quantum OTOC exhibits an oscillatory behavior with time, and the initial time interval in which the OTOC grows tends to be different from the Ehrenfest time as studied in previous work [74]. It is necessary to redefine the short time scale as one beyond which the oscillatory behavior starts, which we call the revival time t_R. For classical integrable systems, this time can be calculated analytically (Appendix C). Especially, for the Dirac circular billiard, the revival time is $t_R \approx 4$ while that for the Schrödinger counterpart we have $t_R \approx 1.3$. To enable a meaningful comparison, we define the small time regime as $t < 1$.

For physical systems at a finite temperature, thermal fluctuations are important. It is thus necessary to incorporate thermal average to calculate the OTOC time evolution [72]. Expanding OTOC in the energy eigenspace of the billiard system and imposing the thermal averaging:

$$c_n(t) = \langle n| - [\widehat{W}(t), \widehat{V}(0)]^2 |n\rangle, \tag{3}$$

we obtain the *canonical* expectation value of the OTOC as [68,74]

$$C_T(t) = \frac{\sum_n c_n(t)\exp(-E_n/T)}{\sum_n \exp(-E_n/T)}, \tag{4}$$

where $C_T(t)$ depends on both temperature T and time t. Note that $c_n(t)$ represents the *microcanonical* evolution.

To be concrete, we focus on the time dependence for a given temperature. Because of the characteristically different energy-momentum dispersion relation in the Schrödinger and Dirac billiards, the energy scales in the two types of systems are different by several orders of magnitude. For each system, we choose the temperature T to correspond to the 100th eigenenergy, so that using the first 1000 eigenmodes in the summation in Eq. (4) can guarantee high accuracy. For the Schrödinger billiards, all eigenenergies are positive. For the Dirac billiards, there are both positive and negative eigenenergy values, corresponding to particle and hole states, respectively. In this case, to sample the whole Hilbert space, it is necessary to include a sufficient number of both particle and hole states. For the purpose of revealing any symmetric patterns in the microcanonical evolution of OTOC, for the negative energy states we use the absolute values of the energies.

Fig. 2 presents the main results for the short time evolution of OTOC for the integrable and chaotic, Schrödinger and Dirac billiard systems. Specifically, For the Schrödinger case, the microcanonical OTOC for the circular billiard exhibits high frequency oscillations, as shown in Fig. 2(a). These oscillations occur because the underlying system is integrable, for which there are a large number of commensurate eigenenergies [68,74]. For the chaotic billiard, the eigenenergies are incommensurate, so no such oscillations occur, as shown in Fig. 2(b). The evolution of the canonical OTOC for the Schrödinger case is shown in Fig. 2(c) and (d) for the integrable and chaotic billiards, respectively. The initial growth is not exponential but somewhat algebraic, regardless of

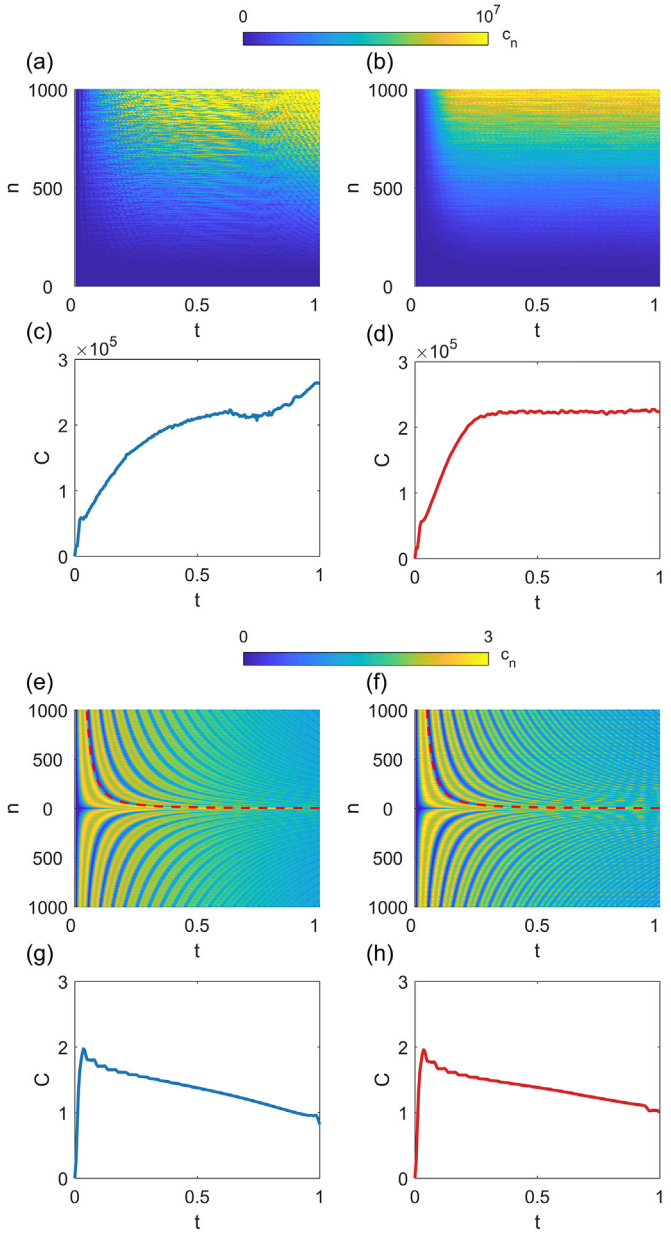

Fig. 2. *Short time evolution of OTOC in Schrödinger and Dirac billiard systems.* Panels (a,b,e,f) show the short time evolution of the microcanonical OTOC (color coded) for the first 1000 energy eigenstates, and panels (c,d,g,h) display the evolution of the canonical OTOC. Panels (a–d) and (e–h) are for the Schrödinger and Dirac billiard systems, respectively. Panels (a,c,e,g) are for the integrable circular billiard, while panels (b,d,f,h) are for the chaotic African billiard. For the Schrödinger billiards, the quantity $\partial\widehat{H}/\partial\widehat{p}$ depends on $\widehat{p}$ so that the OTOC values are orders of magnitude larger than those in the Dirac billiards. In the Schrödinger case, the short time evolution of the canonical OTOC exhibits characteristically different behaviors [c.f., panels (c) and (d)], depending on whether the corresponding classical dynamics are integrable or chaotic. The Dirac billiards exhibit no such difference [c.f., panels (g) and (h)], indicating suppression of manifestations classical chaos. The uniquely relativistic quantum phenomenon of Zitterbewegung is pronounced, which can be seen in panels (e) and (f), regardless of the nature of the underlying classical dynamics. The red dashed curves in (e) and (f) indicate the period of the Zitterbewegung motion as a function of the eigenenergy: the period is large for small energy values but decreases quickly as the energy is increased.

the nature of the classical dynamics. However, for the integrable billiard, the growth is largely monotonic, but for the chaotic billiard, even within the short time scale considered, the growth saturates. This is then the characteristic difference between the short time growth behaviors for the integrable and chaotic billiards, which can be attributed to the difference in the microcanonical evolution of OTOC: for the former there are oscillations [Fig. 2(a)], while no oscillations occur for the latter [Fig. 2(b)].

For the Dirac billiards, Fig. 2(e) and (f) show the evolution of the microcanonical OTOC for the integrable and chaotic billiards, respectively, which exhibit a strong similarity. The corresponding evolution of the canonical OTOC is shown in Fig. 2(g) and (h). For both the microcanonical and canonical OTOC, the short time evolution gives no fingerprint of classical chaos, indicating that chaos has been suppressed by the strong relativistic quantum effects. In fact, a uniquely relativistic quantum phenomenon, Zitterbewegung motion [94], appears unequivocally in Fig. 2(e) and (f), where the red dashed lines give the period of Zitterbewegung oscillations as a function of the eigenenergy, for both the particle and hole states. For a massless Dirac electron, when the absolute value of the energy is close to zero, the Zitterbewegung period is large [95]. As the absolute energy value is increased, the period decreases rapidly. The physical origin of Zitterbewegung is the interference between the particle and hole states [6,94]. In particular, due to the particle-hole symmetry, if $\boldsymbol{\psi}_n = (\psi_1, \psi_2)^T$ is an eigenspinor of $\widehat{H}$ with energy E (particle), then $\boldsymbol{\psi}_{-n} = (\psi_2^*, \psi_1^*)^T$ is also an eigenspinor with the negative energy $-E$ (hole) [6]. The similarity in the spinor wavefunctions associated with the particle and hole states generates a large expectation value for an operator, giving rise to the observed high frequency oscillations. The particle-hole picture also explains the suppression of chaos in the Dirac billiards [Fig. 2(e,g) versus Fig. 2(f,h)]: due to the linear dispersion relation, in the first-order approximation, the particle-hole symmetry dominates (Appendix D), weakening or even eliminating any features of the underlying classical dynamics including chaos.

The short time behaviors of OTOC with respect to the nature of the classical dynamics can be summarized, as follows. For the Schrödinger billiards, before the first revival time, there are signatures of chaos in the microcanonical and canonical evolution of OTOC. However, for the Dirac billiards, chaos is suppressed by the relativistic quantum effects so that the evolution of OTOC gives no indication of classical chaos.

4. Long time evolution of the OTOC

In the long time regime defined by $t > t_R$, quantum effects in the evolution of OTOC become more and more pronounced. While the focus of most previous work on OTOC was on possible detection of any quantum exponential growth behavior, i.e., the butterfly effect, in the short time regime [64–76], there was also work on the long time behavior of OTOC [68,74,96,97]. A remarkable phenomenon is the emergence of oscillations in nonrelativistic quantum OTOC evolution for classically integrable systems [68,74,96]. Our goal here is to detect and examine any possible oscillatory behaviors in relativistic quantum evolution of OTOC.

For convenience, we normalize the time by the revival time t_R, so the long time regime becomes $t \gg 1$. Before discussing the dynamical evolution of OTOC, it is necessary to investigate the effect of finite temperature on evolution. For this purpose, we normalize the canonical OTOC C_T by dividing by the following temperature-dependent factor [67,71,72,91]:

$$\overline{C}_T = \langle \widehat{W}(t)\widehat{V}\widehat{V}\widehat{W}(t) + \widehat{V}\widehat{W}(t)\widehat{W}(t)\widehat{V}\rangle_T$$

to obtain

$$C_T \Big/ \overline{C}_T = 1 - \frac{\tilde{C}_T}{\overline{C}_T} \approx 1 - \frac{\langle \widehat{W}(t)\widehat{V}\widehat{W}(t)\widehat{V} + \widehat{V}\widehat{W}(t)\widehat{V}\widehat{W}(t)\rangle_T}{2\langle \widehat{W}\widehat{W}\rangle_T \langle \widehat{V}\widehat{V}\rangle_T}. \tag{5}$$

where the out-of-time component of OTOC is

$$\tilde{C}_T = \langle \widehat{W}(t)\widehat{V}\widehat{W}(t)\widehat{V} + \widehat{V}\widehat{W}(t)\widehat{V}\widehat{W}(t)\rangle_T.$$

A general discussion and a physical understanding of the temperature dependence of OTOC evolution are presented in Appendix B.

Fig. 3(a) and (b) show the evolution of the temperature normalized OTOC for the Schrödinger billiards into the long time regime $0 \le t \le 10$ and in the asymptotically long time regime $46 \le t \le 50$, respectively, where the blue and red traces are for the integrable and chaotic billiards, respectively. Except for an initial short time period ($t \lesssim 0.5$), the behaviors of OTOC evolution for the integrable and chaotic billiards are characteristically different. In particular, for the circular billiard, there are persistent oscillations (fluctuations) in the OTOC with a slowly decaying amplitude [68]. However, for the chaotic billiard, in spite of small random fluctuations, OTOC becomes largely saturated. The approximately constant OTOC value in the long time regime is an unequivocal signature of classical chaos in nonrelativistic quantum systems.

In the relativistic quantum system, however, the behavior of the long time evolution of OTOC for the chaotic billiard is quite different from that in the nonrelativistic quantum counterpart, as shown in Fig. 3(c). Specifically, in the time interval examined, OTOC exhibits large amplitude oscillations, regardless of whether the classical dynamics are

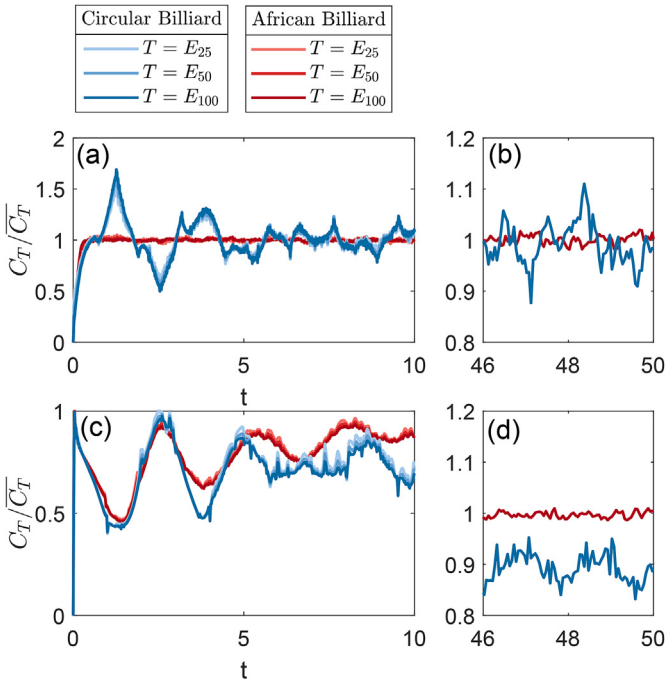

Fig. 3. *OTOC evolution in the long time regime for integrable and chaotic billiards at different temperatures.* (a,b) For the Schrödinger billiards, evolution of the temperature normalized OTOC $C_T/\overline{C}_T$ in the time interval $0 \le t \le 10$ and $46 \le t \le 50$, respectively, where the blue and red traces are for the circular and African billiard, respectively. For the integrable billiard, oscillations of OTOC extend into the long time regime, regardless of temperature. For the chaotic billiard, OTOC tends to saturate quickly into an approximately constant value with small random fluctuations, which is characteristically different from the behavior of the integrable billiard and can be regarded as a (nonrelativistic) quantum manifestation of classical chaos. (c,d) The corresponding evolution for the Dirac billiards. Asymptotically, e.g., in the time interval $46 \le t \le 50$, the OTOC oscillations persist for the integrable billiard but they diminish for the chaotic billiard. While this behavior is qualitatively similar to that in the Schrödinger billiards, in the time interval $0 \le t \le 10$, a quite different feature arises: the normalized OTOC exhibits large oscillations for the Dirac billiards, regardless of the nature of the classical dynamics. This means that, in the long but not asymptotically long time regime, the effect of chaos is suppressed in the relativistic quantum billiard as compared with that in the nonrelativistic quantum billiard. In all cases, temperature has little effect on the OTOC evolution.

integrable or chaotic. In fact, there is no signature of chaos in the OTOC evolution, i.e., chaos is suppressed in the relativistic quantum billiard. We note that, a signature of chaos does tend to arise but only in the asymptotically long time regime, as shown in Fig. 3(d), where the OTOC tends to an approximately constant value, similar to the behavior in the nonrelativistic quantum billiard in Fig. 3(b). That is, the effects of chaos kick in but only in the asymptotically long time regime. Overall, a comparison between Fig. 3(a) and (c) gives the unmistakable message that, in the long time regime, the laws of relativistic quantum mechanics make the signatures of classical chaos much less pronounced as compared with the laws of nonrelativistic quantum mechanics.

To probe further into the difference between OTOC evolution of the integrable and chaotic billiards, we examine the structure of the oscillations in detail in the semiclassical regime, where a quantum particle can be viewed as a wave packet. A Gaussian wave packet initially placed in the billiard domain will spread. If the billiard dynamics are classically integrable, there will come a time at which the wave packet is revived [98] - the revival time t_R. To gain insights into this phenomenon, we calculate the revival frequencies for three types of integrable systems, as listed in Table 1. To compare the values of the revival frequencies with the ones of OTOC oscillations, we perform a Fourier analysis of OTOC time evolution, as shown in Fig. 4(a) and (c) for the Schrödinger and Dirac billiards, respectively. For both the circular Schrödinger and Dirac billiards, the revival frequency is approximately the value determined by twice the classical revival period, due to the square of the operators in the OTOC definition.

The difference in the long time evolution of OTOC in the Schrödinger billiards with integrable and chaotic dynamics can be understood by noting that, for an integrable system, an initial wave packet will recur in the course of evolution. While recurrence can be perfect for simple 1D systems such as the quantum harmonic oscillator or the 1D infinite potential well system, for the circular billiard, a recurred wave packet will not be exactly identical to the initial wave packet but involve a number of angular momentum channels [99]. Especially, the quantities $c_n(t)$ in Eq. (3) for different values of n possess different frequencies, ruling out the possibility of any perfect recurrence in C_T. For a chaotic billiard, recurrences are unlikely [80], because an initially localized wave packet will typically spread, involve in principle all possible quantum channels, and distribute uniformly in the physical space. This can also be seen in Fig. 4(a), where the Fourier spectrum of OTOC of the chaotic billiard exhibits no dominant peak. As a result, OTOC tends to an approximately constant value after an initial growth.

The revival behavior in the time evolution of the OTOC can also be analyzed using the approach of $1/f$ noise scaling, a useful tool in the study of quantum chaos [100–102]. In particular, we introduce the following difference in $C_T(t)$:

$$s_i = C_T(t_i + \Delta t) - C_T(t_i) \tag{6}$$

where Δt is a small time interval. The spectral fluctuation of the sequence $\{s_i\}$ is given by $\delta_n = \sum_{i=1}^{n}(s_i - \langle s\rangle)$. The Fourier transform of δ is

Table 1
Revival periods of classical motion and the OTOC. Abbreviations: 1DIPW - one-dimensional infinite potential well, CSB - circular Schrödinger billiard, CDB - circular Dirac billiard.

System	Eigenvalue	Revival Period	OTOC Period
1DIPW	$E_n = \frac{n^2\pi^2\hbar^2}{2mL^2}$	$\frac{4mL^2}{\pi\hbar}$ (Revival)	$\frac{2mL^2}{\pi\hbar}$
CSB	$E_n \approx \frac{\hbar^2\pi^2}{2mR^2}\left(n+\frac{\lvert l\rvert}{2}+\frac{3}{4}\right)^2$	$\frac{8mR^2}{\hbar\pi}$ ($l=0$ Revival)	$\frac{16mR^2}{\hbar\pi}$
		$\frac{40mR^2}{\hbar\pi}$ ($l\neq 0$ Revival)	
CDB	$E_n \approx \frac{\pi v_F n}{2R}$	$\frac{4R}{v_F}$ (Classical motion)	$\frac{2R}{v_F}$

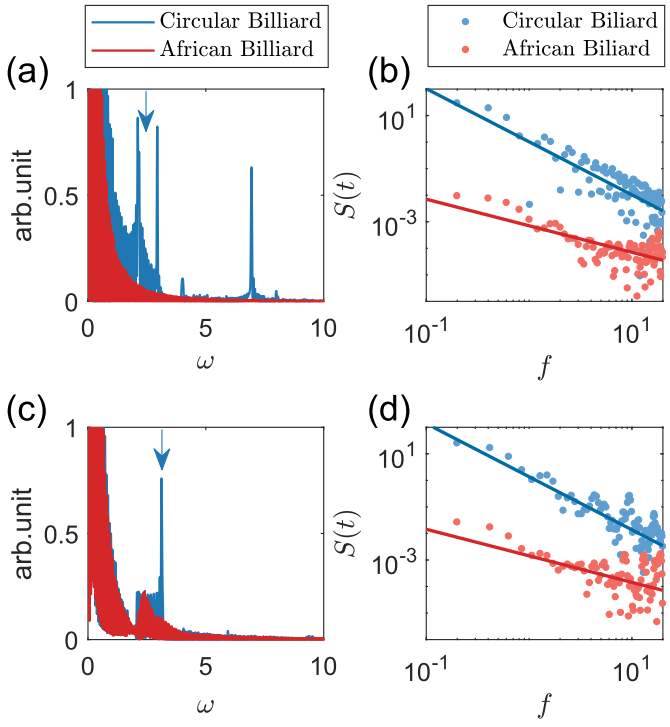

Fig. 4. Revival frequency of OTOC oscillations and $1/f$ noise. (a) Blue trace: Fourier transform of OTOC time evolution for the Schrödinger circular billiard for $t \in [0, 100]$. The arrow indicates the frequency determined by twice the classical revival period. The splitting is due to the quadratic relationship between energy and momentum. For comparison, the Fourier spectrum of the OTOC time evolution of the Schrödinger African billiard is included (the red trace), where there is absence of any pronounced peak. (b) Scaling of $1/f$ noise spectrum for $t \in [50, 100]$. For the circular billiard, the scaling exponent is approximately $\gamma = 2$ (blue fitting line). For the African billiard, the exponent is approximately $\gamma = 1$ (red fitting line). (c,d) Results corresponding to those in (a,b), respectively, but for the Dirac billiards. The values of the scaling exponent are similar to those in (b).

$$\widehat{\delta}_f = \sum_n \delta_n \exp\left(\frac{-2\pi i f n}{N}\right), \tag{7}$$

with the power spectrum given by

$$S(f) = |\widehat{\delta}_f|^{2\sim} 1/f^{\gamma}, \tag{8}$$

where γ is the $1/f$ scaling exponent. For integrable and chaotic billiards, the prediction is [100–102] $\gamma = 1$ and $\gamma = 2$, respectively. Numerical results are shown in Fig. 4(b) and (d), where the $1/f$ noise analysis is carried out in the time interval $t \in [50, 100]$ (after a dozen revivals for the integrable billiard). While the theoretical prediction [100–102] was obtained for nonrelativistic quantum billiard, we find that the same scaling law holds for the relativistic quantum billiards, as demonstrated in Fig. 4(d), suggesting the generality of the $1/f$ scaling analysis.

5. OTOC based on wave packet evolution

The evolution of the wave packet is key to understanding the oscillatory behavior of OTOC as presented in Sec. 4. For a Gaussian wave-packet initially placed in a billiard system, its time evolution can reveal the nature of the corresponding classical dynamics, as exemplified by the previous work on Loschmidt echo [103] in quantum billiards with a random potential. The issue of wave packet revival was extensively studied [98]. It was also found that the linear dispersion in relativistic quantum systems tends to suppress wave-packet spreading in periodic quantum transport systems [104,105]. In general, examining the

evolution and behavior of the wave packet can lead to richer information about the system than merely the eigen wavefunctions.

As an alternative to the energy eigenstate based approach in Eq. (3), here we develop a wave packet based approach to calculating OTOC to gain more physical insights. Straightforwardly, instead of taking the average with respect to the energy eigenstates, we use the following wave-packet average of the OTOC operator [74,76]:

$$C_0 = \langle\psi_0|C^2(t)|\psi_0\rangle, \tag{9}$$

and proceed to calculate the so-defined OTOC for all cases treated in Sec. 4 (integrable and chaotic, nonrelativistic and relativistic quantum). Specifically, for the Dirac billiards, we choose the wave packet as

$$\psi_0 = N\exp\left(-\frac{(\mathbf{r}-\mathbf{r}_0)^2}{2\xi^2} + i\mathbf{k}\cdot\mathbf{r}\right)\begin{pmatrix} a \\ b \end{pmatrix}. \tag{10}$$

where ξ is the width of the wave packet and N is a normalization constant. We choose $a = \sqrt{2}/2$ and $b = \sqrt{2}/2\exp(i\varphi)$ (with $a^2 + b^2 = 1$). For simplicity, we set $\varphi = \pi/4$. For the Schrödinger billiards, the wave packet has the same form except that the two-component spinor $\begin{pmatrix} a \\ b \end{pmatrix}$ is removed. A typical numerical setting is $\mathbf{r}_0 = 0$, $\xi = 0.1$ and $k = 20$. The result has also been verified with different initial conditions. The Ehrenfest time is estimated by the width of the wave packet when it reaches the system size. For the circular billiard, the theoretically estimated Ehrenfest time [74] is $t_E \approx \xi = 0.1$.

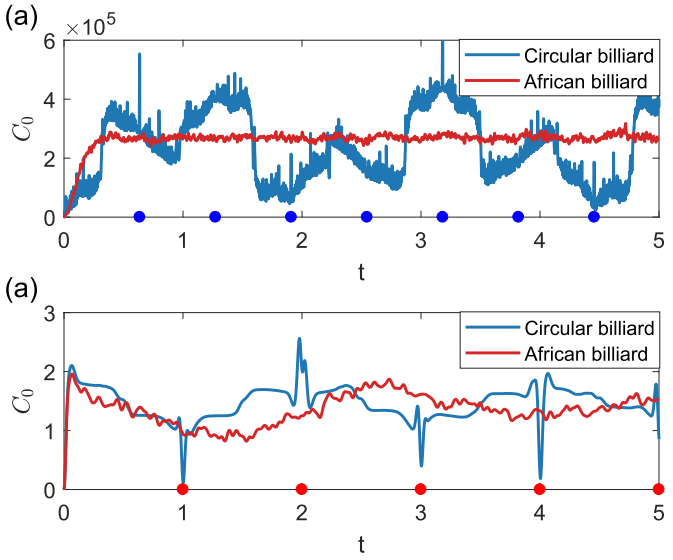

Fig. 5. *Time evolution of the wave packet based OTOC in integrable and chaotic, Schrödinger and Dirac billiards.* (a) For the Schrödinger billiard, OTOC C_0 defined in terms of the wave packet versus time, where the blue and red traces are for the integrable and chaotic billiard, respectively. The time between two adjacent blue dots is half of the revival time of the corresponding classical motion. Similar to the evolution of the eigenstate based OTOC, there is a characteristic difference between the wave packet based evolution of OTOC for the integrable and chaotic billiards: there are oscillations in the former while the latter tends rapidly to a constant value (as a pronounced signature of classical chaos). (b) The results for the Dirac billiard, where the OTOC exhibits oscillations regardless of the nature of the classical dynamics. The time between two adjacent red dots is one fourth of the revival time of the classical motion. Similar to the result in Fig. 2(b), chaos is suppressed in this relativistic quantum billiard system.

Fig. 5(a) and (b) show the time evolution of C_0 for the Schrödinger and Dirac billiards, respectively. Similar to Fig. 3(a), for the Schrödinger case, Fig. 5(a) shows that the behaviors of C_0 are characteristically different for the integrable and chaotic billiards, indicating a distinct quantum manifestation of classical chaos. However, for the Dirac case, the difference is largely absent, as shown in Fig. 5(b), implying suppression of chaos. Note that the results in Fig. 5(b) are quite consistent with those in Fig. 3(b). A minor difference between the wave-packet based and the eigenstate based evolution of OTOC is that, in the former there are occasional, sharp changes that are particular pronounced for the integrable billiards, which are caused by the bounces of the wave packet at the billiard boundary.

6. Level spacing distribution of the OTOC operator in integrable and chaotic billiards

The statistical distributions of energy level spacing are perhaps one of the most studied topics in nonrelativistic quantum chaos [2–4]. An established result is that the energy level spacing follows statistically distinct distributions for integrable and chaotic systems [2–4] as described by those of the Poisson and GOE random matrices, respectively. A remarkable signature of classical chaos in the distribution is level repulsion as stipulated by the Wigner distribution for GOE random matrices [106,107]. Experimental tests of the random matrix based prediction were conducted using microwave cavities [108,109]. In relativistic quantum chaotic systems such as graphene and Dirac billiards, the energy level spacing distributions have also been studied [12,110–112], with unconventional phenomena such as the occurrence of GOE statistics in classical integrable graphene billiard systems [112].

A natural question is whether the eigenvalues of the OTOC operators $\langle C^\alpha\rangle$ would exhibit statistically distinct distributions for integrable and chaotic systems. In two recent studies [113,114], the connection between the Sachdev-Ye-Kitaev (SYK) model and random matrix theory in terms of OTOC was considered, where the characteristics of the Gaussian ensemble depend on the particle number [113,114]. Another recent work [115] reported universal level statistics of OTOC operator for Schrödinger systems. Here we calculate the OTOC level spacing statistics for Dirac billiards with integrable and chaotic classical dynamics and compare the results with those from the Schrödinger counterparts.

We expand the OTOC operator C^α in the energy eigenspace to obtain the matrix $\langle C^\alpha\rangle$, whose eigenvalues can then be calculated. Because of the symmetry between the positive and negative eigenvalues, it suffices to focus on the positive ones. Following the definition of quantum Lyapunov spectrum [115,116], we resort to a logarithmic scale and calculate the quantity $\log\Lambda^+$, where Λ^+ is the positive eigenvalue of $\langle C^\alpha\rangle$, and extract the level spacing accordingly. We take the OTOC operators at sufficiently long time to remove any initial transient behavior and ensure that the level spacing statistics change little when longer time intervals are used.

Fig. 6(a) and its inset show the level spacing distributions for $\alpha = 2$ and $\alpha = 1$, respectively, for Schródinger billiard systems. In both cases, the black and blue zigzagged curves are for the integrable and chaotic billiards, respectively. As explained in the caption of Fig. 6, the level spacing distributions are Poisson and GOE for the integrable and chaotic billiards, respectively, which are essentially the same as those of the energy level spacing [2–4]. We see that, for nonrelativistic quantum billiard systems, the level spacing distributions of the OTOC operators bear an unequivocal signature of classical chaos.

The situation is quite different for the Dirac billiards. For a chaotic billiard, if the value of α is an even (odd) integer, time reversal symmetry is preserved (broken), so that the level spacing distribution should follow

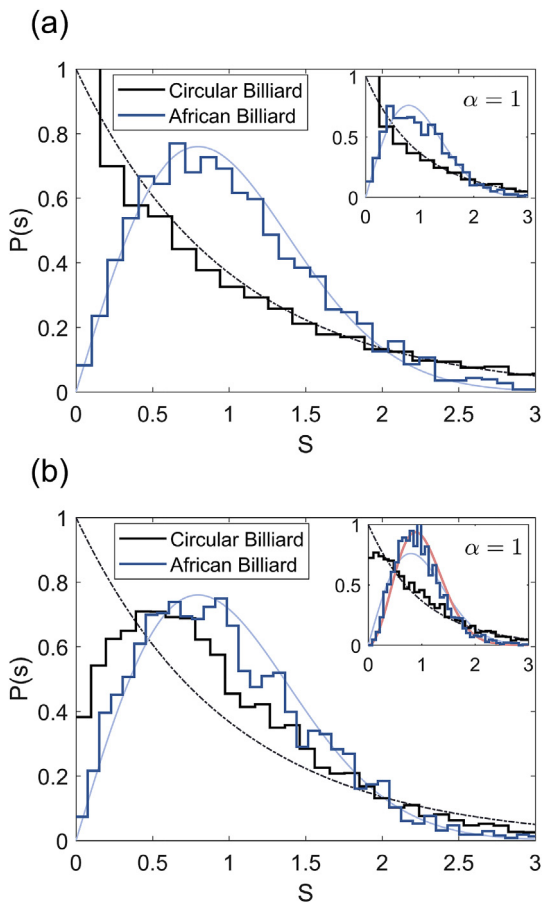

Fig. 6. *Level spacing distributions of OTOC operator C^{α} for nonrelativistic and relativistic quantum billiards*. (a) The level spacing distributions of C^2 for the Schrödinger integrable (zigzagged solid black curves) and chaotic (zigzagged solid blue curves) billiards. The smooth black dashed and smooth blue curves represent the Poisson and GOE distribution, respectively. The reasonably good fittings between the zigzagged curves and their corresponding smooth curves mean that, for the classical integrable billiard, the level spacing distribution is Poisson while that for the chaotic billiard is GOE. Qualitatively similar results hold for $\alpha = 1$ (inset). All these results indicate a strong signature of classical chaos in altering the characteristics of the level spacing distribution in nonrelativistic quantum systems. (b) The corresponding results for the Dirac billiards. For $\alpha = 2$, the level spacing distribution for the integrable billiard lies between those of Poisson and GOE. Because of the even value of α, time reversal symmetry is reserved, so the distribution for the chaotic billiard is still GOE. Comparing with the distributions for the corresponding Schrödinger case, the difference between those of integrable and chaotic billiards is significantly reduced, implying suppression of chaos in the relativistic quantum systems. If the value of α is odd, time reversal symmetry is broken. In this case, for the chaotic billiard, the level spacing distribution is of the GUE type (inset).

that of GOE (GUE). We have verified that this is indeed the case for $\alpha = 1, 2, 3$ and 4. As shown in Fig. 6(b) and explained in its caption, the difference in the level spacing distribution between the integrable and chaotic billiards is less pronounced as compared with that in the Schrödinger case, suggesting that chaos is suppressed by relativistic quantum effects. This result is consistent with those from the time evolution behaviors of OTOC in Secs. 3 and 4, as well as with that based on the wave packet evolution in Sec. 5.

7. Discussion

A number of recent studies have suggested that OTOC can be a promising framework in the traditional field of nonrelativistic quantum chaos for detecting possible exponential sensitivity and probing more deeply into the quantum manifestations of classical chaos [64,67,69–76]. This paper presents a systematic study of OTOC in relativistic quantum systems, with the take-home message that the signatures of classical chaos in relativistic quantum systems are less pronounced than in nonrelativistic quantum systems. We have obtained this conclusion through a comprehensive, multi-angle approach in terms of four different aspects of OTOC: short time and long time evolution in the energy eigenspace, wave-packet based evolution, and level spacing statistics. In particular, we introduce and justify a time scale, the revival time, to separate the short from long time regime. Firstly, in the energy eigenspace of the Hamiltonian, the short time evolution behaviors of the nonrelativistic quantum OTOC are characteristically distinct for classically integrable and chaotic billiards, while those of the relativistic quantum OTOC exhibit no apparent difference, indicating a suppression of the effects of chaos. In fact, for the latter, uniquely relativistic quantum behaviors such as negative energy states and Zitterbewegung motion are pronounced especially in the short time regime [Fig. 2(e and f)], but the remarkable phenomenon is that these behaviors, even in minuscule details, appear essentially the same for classically integrable and chaotic dynamics. Secondly, in the long time regime, for the Schrödinger billiards, the characteristic difference in the OTOC evolution of the integrable and chaotic billiards persists, while those in the Dirac integrable and chaotic billiards still exhibit qualitatively similar behaviors [Fig. 3(a, c)]. In fact, for the former, a drastic difference in OTOC evolution sets in almost immediately after the system evolution starts [Fig. 3(a)], but for the latter, a noticeably characteristic difference appears but only in the asymptotic time regime [Fig. 3(d)], implying much weaker manifestations of classical chaos in the relativistic quantum than in nonrelativistic quantum systems. Thirdly, wave-packet based OTOC evolution exhibits essentially the same phenomenon (Fig. 5), reinforcing the finding that the relativistic quantum machinery tends to suppress the fingerprints of classical chaos more than the nonrelativistic quantum one. Finally, the level spacing statistics of OTOC in the Schrödinger billiards are similar to those of the energy Hamiltonian in that integrable dynamics lead to the Poisson distribution while classical chaos gives rise to distributions characteristic of GOE random matrices - one of the best established results in the field of quantum chaos [2–4]. In the Dirac systems, while the level spacing distributions of a chaotic billiard can be those of GOE or GUE (depending on whether the order of the OTOC operator is even or odd), the differences in the distributions between the classically integrable and chaotic dynamics are markedly less pronounced than in the corresponding Schrödinger systems (Fig. 6).

Declaration of Competing Interest

There is no conflict of interest.

Acknowledgments

We would like to acknowledge support from the Vannevar Bush Faculty Fellowship program sponsored by the Basic Research Office of the Assistant Secretary of Defense for Research and Engineering and funded by the Office of Naval Research through Grant No. N00014-16-1-2828. LH is supported by NNSF of China under Grants No. 11775101 and No. 11422541.

Appendix A. Matrix representation of OTOC

Appendix A.1. Nonrelativistic quantum billiard systems

The Schrödinger Hamiltonian is

$$\widehat{H} = \frac{\widehat{\mathbf{p}}^2}{2m} + V(\mathbf{r}), \tag{A.1}$$

where $V(\mathbf{r})$ is the potential field that defines the billiard. Using the commutation relation $\widehat{p}_x = (i/2)[\widehat{H}, \widehat{x}]$, we can construct the matrix $\langle \widehat{p}_x \rangle$ from $\langle \widehat{x} \rangle$. The elements of the two matrices are related to each other through

$$p_{mn} = \frac{i}{2}(E_m - E_n)x_{mn}. \tag{A.2}$$

For a 1D infinite potential well of width L, the matrix elements x_{nm} are given by Ref. [74].

$$x_{nm} = \begin{cases} \dfrac{L}{2} & (n = m), \\ \dfrac{1-(-1)^{n+m}}{\pi^2} L\left[\dfrac{1}{(n+m)^2} - \dfrac{1}{(n-m)^2}\right] & (n \neq m), \end{cases} \tag{A.3}$$

which leads to

$$\lim_{n\to\infty} x_{mn} \sim \frac{1}{n^3}, \text{ and } \lim_{n\to\infty} p_{mn} \sim \frac{1}{n}. \tag{A.4}$$

Since the energy eigenfunctions of the 1D infinite potential well systems are sinusoidal functions, Eq. (A.4) gives $\int x \sin(nx)\sin(mx)dx \sim 1/n^3$ and $\int \sin(nx)\sin(mx) \sim 1/n$.

For the circular billiard of unit radius, the solutions of the Schrödinger equation are

$$\psi_{ls} = N_{ls} J_l(k_{ls} r)\exp(il\theta), \tag{A.5}$$

where k_{ls} denotes the sth zero point of the lth order Bessel function and N_{ls} is the normalization constant. We thus have

$$x_{lsl's'} = \begin{cases} \int_0 \pi r^2 J_l(k_{ls} r) J_{l'}(k_{l's'} r)\, dr, & |l - l'| = 1, \\ 0, & \text{others.} \end{cases} \tag{A.6}$$

To simplify the eigen wavefunctions, we use the Weyl formula [2,6].

$$N(k) = \frac{Ak^2}{4\pi} + \gamma\frac{Lk}{4\pi}, \tag{A.7}$$

where $N(k)$ is the number of eigenvalues below k, A and L are the area and perimeter of the billiard, respectively, γ is a constant that depends on the boundary condition. For large k values, we thus have $N \sim E$. Using the asymptotic expansion of the Bessel function [117].

$$J_l(x) \sim \sqrt{\frac{2}{\pi x}}\cos\left(x - \frac{1}{2}l\pi - \frac{1}{4}\pi\right), \tag{A.8}$$

we have that, for any given quantum number (l,s), the nonzero values of $x_{lsl's'}$ are determined by $(l \pm 1, s')$, indicating that the values of s' can be large for $n \to \infty$. Using the asymptotic expansion and integral (which give $x(m, n^2) \sim 1/n^3$) for the 2D circular Schrödinger billiard, we have

$$\lim_{n\to\infty} x_{mn} \sim \frac{1}{n^{3/2}}, \text{ and} \tag{A.9}$$

$$\lim_{n\to\infty} p_{mn} \sim \frac{1}{n^{1/2}}. \tag{A.10}$$

Appendix A.2. Relativistic billiard systems

For a Dirac system, the commutation relation is

$$1/2(\widehat{H}\widehat{\sigma}_x + \widehat{\sigma}_x\widehat{H}) = \widehat{p}_x.$$

We can construct the matrix elements $\langle \widehat{p}_x \rangle$ from $\langle \widehat{\sigma}_x \rangle$ as

$$p_{mn} = \frac{1}{2}\sigma_{mn}(E_m + E_n). \tag{A.11}$$

For a circular billiard, the solution of the Dirac equation is

$$\boldsymbol{\psi}_{ls} = N_{ls}\begin{pmatrix} J_l(k_{ls}r) \\ iJ_{l+1}(k_{ls})\exp(i\theta) \end{pmatrix}\exp(il\theta), \tag{A.12}$$

where k_{ls} is determined by the boundary condition $J_l(k_{ls}) = J_{l+1}(k_{ls})$. The current operator is

$$\sigma_x = \begin{pmatrix} 0 & 1 \\ 1 & 0 \end{pmatrix}. \tag{A.13}$$

The particle-hole symmetry stipulates that, for any potential $V(\mathbf{r})$, if $|p\rangle = (\psi_1, \psi_2)^T$ is a solution of the Dirac equation with energy E, then $|h\rangle = (\psi_2^*, \psi_1^*)^T$ is a solution with energy $-E$. Using both the particle and hole states, we construct the matrix $\langle\sigma_x\rangle$ as

$$\langle\sigma_x\rangle = \begin{bmatrix} \langle p|\sigma_x|p\rangle & \langle p|\sigma_x|h\rangle \\ \langle h|\sigma_x|p\rangle & \langle h|\sigma_x|h\rangle \end{bmatrix} = \begin{bmatrix} PP_{mn} & PH_{mn} \\ HP_{mn} & HH_{mn} \end{bmatrix}. \tag{A.14}$$

The nonzero matrix elements are given by

$$\begin{aligned} PP_{lsl's'} &= -2\pi i\int rJ_{l+1}(k_{ls}r)J_{l'}(k_{l's'}r)dr \text{ for } (l-l' = -1), \\ PP_{lsl's'} &= 2\pi i\int rJ_l(k_{ls}r)J_{l'+1}(k_{l's'}r)dr \text{ for } (l-l' = 1), \\ HP_{lsl's'} &= 2\pi\int rJ_l(k_{ls}r)J_{l'}(k_{l's'}r)dr \text{ for } (l+l' = 0), \\ HP_{lsl's'} &= -2\pi\int rJ_{l+1}(k_{ls}r)J_{l'+1}(k_{l's'}r)dr \text{ for } (l+l' = -2), \\ HH_{lsl's'} &= PP^*_{lsl's'}. \end{aligned} \tag{A.15}$$

Using the integral $\int \sin(nx)\sin(mx)\sim 1/n$ and Eq. (A.8), we have

$$\lim_{n\to\infty} PP_{mn} \sim \frac{1}{\sqrt{n}}. \tag{A.16}$$

Using the Weyl formula Eq. (A.7) and the dispersion relation $E\propto k$ for massless Dirac systems, from the relationship Eq. (A.11), we can show

$$\lim_{n\to\infty} p_{mn} \to \text{constant},$$

so the square OTOC operators cannot be defined for the Dirac billiards.

Appendix B. Temperature dependence

The OTOC defined in Eq. (1) for $\alpha = 2$ can be expanded as

$$\begin{aligned} -\langle[\widehat{W}(t), \widehat{V}(0)]^2\rangle_T = &\langle\widehat{W}(t)\widehat{V}\widehat{V}\widehat{W}(t) + \widehat{V}\widehat{W}(t)\widehat{W}(t)\widehat{V}\rangle_T \\ &-\langle\widehat{V}\widehat{W}(t)\widehat{V}\widehat{W}(t) + \widehat{W}(t)\widehat{V}\widehat{W}(t)\widehat{V}\rangle_T, \end{aligned} \tag{B.1}$$

where the first term determines the long time behavior, which is equal to $\langle WW\rangle\langle VV\rangle$. The second term, known as the out-of-time part, exhibits an exponential decay and does not contribute to the long time behavior, which can be used to evaluate the microcanonical averaged OTOC. In particular, in the high temperature limit $T \to \infty$, the expansion coefficient in Eq. (3) is

$$c_n = -\langle\psi_n|[\widehat{W}(t), \widehat{V}(0)]^2|\psi_n\rangle \sim \langle WW\rangle\langle VV\rangle. \tag{B.2}$$

For Schrödinger and Dirac systems, the temperature dependence of the microcanonical averaged OTOC is quite distinct.

Schrödinger system

For a 1D system, we have $E \sim n^2$, which leads to the relation $c_n \sim n^4$ for $\widehat{W} = \widehat{V} = \widehat{p}_x$. Using integration to approximate the summation in Eq. (4), we get

$$C_T = \frac{\int \exp(-E_n/T)c_n dn}{\int \exp(-E_n/T)dn} \sim T^2. \tag{B.3}$$

For a 2D Schrödinger billiard, for $\widehat{W} = \widehat{p}$ and $\widehat{V} = \widehat{p}$, it can be shown that $c_n \sim n^2$ and $C_T \sim T^2$.

For a 2D Schrödinger billiard, for $\widehat{W} = \widehat{x}$ and $\widehat{V} = \widehat{p}$, it can be shown [74] that $c_n \sim n$ and $C_T \sim T$.

Dirac systems

For Dirac billiard systems, we choose $\widehat{W} = \widehat{V} = \widehat{\sigma}_x$, so we have $\lim_{T\to\infty} C_T \sim$ constant.

Appendix C. Wave-packet revival

The revival time can be determined [98,99] from following Taylor expansion of the energy level $E(n)$:

$$E(n) \approx E(n_0) + E'(n_0)(n-n_0) + \frac{E''(n_0)}{2}(n-n_0)^2 + \cdots. \tag{C.1}$$

The time for the onset of periodic motion and the revival time can be obtained in terms of the coefficients $E'(n_0)$ and $E''(n_0)$, respectively, as

$$T_{\rm cl} = \frac{2\pi\hbar}{|E'(n_0)|},\ T_{\rm rev} = \frac{2\pi\hbar}{|E''(n_0)/2|}. \tag{C.2}$$

For an integrable Schrödinger billiard, the dispersion relation for certain angular momentum is $E \sim n^2$. In this case, wave packet revival dominates. For an integrable Dirac billiard, we have $E \tilde{} n$. In this case, periodic motion dominates. Using Eqs. (C.1) and (C.2), we can obtain the revival times for the three types of integrable systems as described in Sec. 4 and presented in Table 1.

Appendix D. Analytic calculation of OTOC in integrable systems

Appendix D.1. Harmonic Oscillator

Equation (1) implies $\widehat{W} = \widehat{V}$ or $\widehat{W} \neq \widehat{V}$. There are two types of OTOC. The case of $C_T = -<[\widehat{x}(t), \widehat{p}(0)]^2>_T$ has been treated in Refs. [73,74]. Here we focus on the case $C_T = -<[\widehat{p}_x(t), \widehat{p}_x(0)]^2>_T$. In the classical limit, we can replace the commutation relation by the Poisson bracket $(\{p_x(t), p_x(0)\}_{\rm P})^2$, where the integration is evaluated over the energy surface. We rewrite the Poisson bracket as

$$\{p_x(t), p_x(0)\}_{\rm P} \sim \frac{\Delta p(t)}{\Delta x(0)}. \tag{D.1}$$

For the quantum harmonic oscillator, in the Heisenberg picture we have

$$\begin{cases} \widehat{x}(t) = \widehat{x}(0)\cos\omega t + \dfrac{1}{\omega}\widehat{p}(0)\sin\omega t, \\ \widehat{p}(t) = \widehat{p}(0)\cos\omega t - \omega\widehat{x}(0)\sin\omega t. \end{cases} \tag{D.2}$$

The commutation relation is then given by

$$\frac{1}{i\hbar}[\widehat{p}_x(t_1), \widehat{p}_x(t_2)] = \omega\sin[\omega(t_1 - t_2)]. \tag{D.3}$$

For classical motion with the initial phase γ, the solution is given by $q(t) = A\cos(\omega t + \gamma)$. The classical growth rate is

$$\int_0^{2\pi} \frac{\delta p(t_1)}{\delta q(t_2)} {\rm d}\gamma = -\omega\sin[\omega({\rm t}_1 - {\rm t}_2)]. \tag{D.4}$$

The minus sign will disappear when taking the square. Thus the classical and quantum cases yield the same result, a special result that holds only for the harmonic oscillator.

Appendix D.2. 1D infinite potential well

We obtain an approximate expression for the thermally averaged OTOC. First, we expand the microcanonical OTOC to get $c_n = \sum_m b_{nm} b^*_{nm}$, where

$$b_{nm} = \langle n|[\widehat{W}(t), \widehat{V}(0)]|m\rangle. \tag{D.5}$$

We then expand b_{nm} in terms of the eigenvectors to get

$$b_{nm} = \sum_\tau \{W_{n\tau}V_{\tau m}\exp[i(E_n - E_\tau)t/\hbar] - V_{n\tau}W_{\tau m}\exp[i(E_\tau - E_m)t/\hbar]\}. \tag{D.6}$$

Equation (D.6) can be regarded as the superposition of many oscillators with the weights proportional to the expectation values of the operator $\widehat{W}$ and $\widehat{V}$. In general, different eigenvectors with similar energy values are coupled strongly, due to the similarity in their wavefunctions.

For the Schrödinger system, we use $C_T = -\langle[\widehat{p}_x(t), \widehat{p}_x]^2\rangle$. For a 1D infinite potential well of width L, the matrix elements x_{nm} can be calculated based on Eq. (A.3). For a large value of n and for $n \neq m$, the first term $1/(n+m)^2$ can be neglected. The second term that contains $1/(n-m)^2$ decays rapidly for $|m-n| \gg 1$. For $m = n, n \pm 1$, we have

$$p_{n,n\pm1} \approx \pm\frac{iL}{\pi^2}2an. \tag{D.7}$$

Substituting Eq. (D.7) into Eq. (D.6) and (B.3) and taking $a = \pi^2\hbar^2/2mL^2$, we obtain

$$c_n(t) = 64n^4\left(\frac{\hbar^4}{4m^2L^2}\right)^2\left[1-\cos\left(\frac{\pi^2\hbar}{mL^2}t\right)\right],$$
$$C_T(t) = \frac{48}{\pi^4}T^2\left(\frac{\hbar^2}{2m}\right)^2\left[1-\cos\left(\frac{\pi^2\hbar}{mL^2}t\right)\right]. \tag{D.8}$$

Using this approximation, we can obtain the dependence of the microcanonical OTOC on n and that of the canonical OTOC on the temperature T. For one period of evolution, we have $T_0 = 2mL^2/\pi\hbar$. From Eq. (C.2), we have that the revival period is given by $T_{re} = 4mL^2/\pi\hbar$, which is twice the OTOC oscillation period.

Appendix D.3. Circular Schrödinger billiard

Following the 1D analysis, we focus on the strongly coupled states with similar energy values in Eq. (A.6). The simplest case is $s = 1$, where the $(l, 1)$ mode couples with the $(l \pm 1, 1)$ modes. For these modes, we have

$$x_{l1l's'} \approx \begin{cases} \text{nonzero}, & \text{for } l' = l \pm 1 \text{ and } s' = 1, \\ 0, & \text{others.} \end{cases} \tag{D.9}$$

For other modes with $l \gg s$, it can be shown that the same oscillation pattern follows but the analysis is more complex. Similarly, for a mode with a large value of l, the frequency depends on Δk_l as

$$\Delta k_l = k_{(l+1)1l1} - k_{l1l1} \approx k_{l1l1} - k_{(l-1)1l1}. \tag{D.10}$$

Using the asymptotic expansion of the Bessel function [117].

$$J_l(x) \sim \sqrt{\frac{2}{\pi x}}\cos\left(x - \frac{1}{2}l\pi - \frac{1}{4}\pi\right). \tag{D.11}$$

we have

$$\Delta k_l = \Delta k = \frac{\pi}{2}. \tag{D.12}$$

A similar argument gives that the period of the OTOC oscillation depends on the quantity $\Delta k^2/\hbar$. We then have

$$T_0 = \frac{16mR^2}{\hbar\pi}, \tag{D.13}$$

where R is the radius of the circular billiard. Note that T_0 is twice the revival time for $l = 0$, approximately half the revival time for $l \neq 0$.

Appendix D.4. Circular Dirac billiard

In the short time regime, Eq. (A.15) indicates that the coupling between the particle states is described by the matrix *PP*. From Eq. (D.9), we obtain the same rule governing the coupling for the Dirac system. The difference from the Schrödinger billiard is the linear dispersion. The terms in Eq. (D.6) then cancel each other.

For the particle-hole states, the coupling is described by the matrix *PH* (*HP*). Consider the microcanonical OTOC c_n, where n denotes the particle state. From Eq. (A.15), we have that the particle-hole states with the same energy will have a large coupling. Equation (D.6) stipulates that this will generate high frequency oscillations with the frequency $\omega = 2|E_n|$ in small time. In fact, the particle-hole symmetry exists, regardless of the nature of the classical dynamics.

In the long time regime, approximated frequency expression cannot be obtained. However, both Figs. 4 and 5 indicate that the frequency can be related to that of the classical wave packet motion.

References

[1] M.C. Gutzwiller, Chaos in Classical and Quantum Mechanics, Springer-Verlag, New York, 1990.
[2] H.-J. Stöckmann, Quantum Chaos: an Introduction, Cambridge University Press, New York, 1999.
[3] F. Haake, Quantum signatures of chaos, in: Springer Series in Synergetics, third ed., Springer-Verlag, Berlin, 2010.
[4] O. Bohigas, M.-J. Giannoni, C. Schmit, Characterization of chaotic quantum spectra and universality of level fluctuation laws, Phys. Rev. Lett. 52 (1) (1984) 1–4.
[5] M.V. Berry, Semiclassical theory of spectral rigidity, Proc. R. Soc. London Series A Math. Phys. Eng. Sci. 400 (1819) (1985) 229–251.
[6] M.V. Berry, R. Mondragon, Neutrino billiards: time-reversal symmetry-breaking without magnetic fields, Proc. R. Soc. Lond. A 412 (1842) (1987) 53–74.
[7] S.W. Mcdonald, A.N. Kaufman, Spectrum and eigenfunctions for a Hamiltonian with stochastic trajectories, Phys. Rev. Lett. 42 (18) (1979) 1189–1191.
[8] E.J. Heller, Bound-state eigenfunctions of classically chaotic Hamiltonian systems - scars of periodic orbits, Phys. Rev. Lett. 53 (16) (1984) 1515–1518.
[9] R.A. Jalabert, H.U. Baranger, A.D. Stone, Conductance fluctuations in the ballistic regime - a probe of quantum chaos, Phys. Rev. Lett. 65 (19) (1990) 2442–2445.
[10] S. Fishman, D.R. Grempel, R.E. Prange, Chaos, quantum recurrences, and Anderson localization, Phys. Rev. Lett. 49 (1982) 509–512.
[11] Y.-C. Lai, H.-Y. Xu, L. Huang, C. Grebogi, Relativistic quantum chaos: an emergent interdisciplinary field, Chaos 28 (5) (2018), 052101.
[12] L. Huang, H.-Y. Xu, C. Grebogi, Y.-C. Lai, Relativistic quantum chaos, Phys. Rep. 753 (2018), 1–128.
[13] A.H.C. Neto, K. Novoselov, Two-dimensional crystals: beyond graphene, Mater. Exp. 1 (2011) 10–17.
[14] P. Ajayan, P. Kim, K. Banerjee, Two-dimensional van der Waals materials, Phys. Today 69 (9) (2016) 38–44.
[15] K.S. Novoselov, A.K. Geim, S.V. Morozov, D. Jiang, Y. Zhang, S.V. Dubonos, I.V. Grigorieva, A.A. Firsov, Electric field effect in atomically thin carbon films, Science 306 (5696) (2004) 666–669.
[16] C. Berger, Z.M. Song, T.B. Li, X.B. Li, A.Y. Ogbazghi, R.F.Z.T. Dai, A.N. Marchenkov, E.H. Conrad, P.N. First, W.A. de Heer, Ultrathin epitaxial graphite: 2D electron gas properties and a route toward graphene-based nanoelectronics, J. Phys. Chem. B 108 (52) (2004) 19912–19916.

[17] K.S. Novoselov, A.K. Geim, S.V. Morozov, D. Jiang, M.I. Katsnelson, I.V. Grigorieva, S.V. Dubonos, A.A. Firsov, Two-dimensional gas of massless Dirac fermions in graphene, Nature 438 (7065) (2005) 197–200.
[18] Y.B. Zhang, Y.W. Tan, H.L. Stormer, P. Kim, Experimental observation of the quantum Hall effect and Berry's phase in graphene, Nature 438 (7065) (2005) 201–204.
[19] A.H.C. Neto, F. Guinea, N.M.R. Peres, K.S. Novoselov, A.K. Geim, The electronic properties of graphene, Rev. Mod. Phys. 81 (1) (2009) 109–162.
[20] N.M.R. Peres, Colloquium: the transport properties of graphene: an introduction, Rev. Mod. Phys. 82 (3) (2010) 2673–2700.
[21] S.D. Sarma, S. Adam, E.H. Hwang, E. Rossi, Electronic transport in two-dimensional graphene, Rev. Mod. Phys. 83 (2) (2011) 407–470.
[22] M.Z. Hasan, C.L. Kane, Colloquium: topological insulators, Rev. Mod. Phys. 82 (2010) 3045–3067.
[23] R. Yang, L. Huang, Y.-C. Lai, C. Grebogi, Quantum chaotic scattering in graphene systems, Europhys. Lett. 94 (2011) 40004.
[24] R. Yang, L. Huang, Y.-C. Lai, L.M. Pecora, Modulating quantum transport by transient chaos, Appl. Phys. Lett. 100 (9) (2012), 093105.
[25] R. Yang, L. Huang, Y.-C. Lai, C. Grebogi, L.M. Pecora, Harnessing quantum transport by transient chaos, Chaos 23 (1) (2013), 013125.
[26] M. Büttiker, Y. Imry, R. Landauer, Josephson behavior in small normal one-dimensional rings, Phys. Lett. A 96 (1983) 365C–367C.
[27] H.-F. Cheung, E.K. Riedel, Y. Gefen, Persistent currents in mesoscopic rings and cylinders, Phys. Rev. Lett. 62 (1989) 587–590.
[28] A. Schmid, Persistent currents in mesoscopic rings by suppression of charge fluctuations, Phys. Rev. Lett. 66 (1991) 80–83.
[29] H. Bouchiat, New clues in the mystery of persistent currents, Physics 1 (2008) 7.
[30] L.P. Lévy, G. Dolan, J. Dunsmuir, H. Bouchiat, Magnetization of mesoscopic copper rings: evidence for persistent currents, Phys. Rev. Lett. 64 (1990) 2074–2077.
[31] V. Chandrasekhar, R.A. Webb, M.J. Brady, M.B. Ketchen, W.J. Gallagher, A. Kleinsasser, Magnetic response of a single, isolated gold loop, Phys. Rev. Lett. 67 (1991) 3578–3581.
[32] D. Mailly, C. Chapelier, A. Benoit, Experimental observation of persistent currents in GaAs-AlGaAs single loop, Phys. Rev. Lett. 70 (1993) 2020–2023.
[33] W. Rabaud, L. Saminadayar, D. Mailly, K. Hasselbach, A. Benoît, B. Etienne, Persistent currents in mesoscopic connected rings, Phys. Rev. Lett. 86 (2001) 3124–3127.
[34] N.A.J.M. Kleemans, I.M.A. Bominaar-Silkens, V.M. Fomin, V.N. Gladilin, D. Granados, A.G. Taboada, J.M. García, P. Offermans, U. Zeitler, P.C.M. Christianen, J.C. Maan, J.T. Devreese, P.M. Koenraad, Oscillatory persistent currents in self-assembled quantum rings, Phys. Rev. Lett. 99 (2007) 146808.
[35] A.C. Bleszynski-Jayich1, W.E. Shanks, B. Peaudecerf, E. Ginossar, F. von Oppen, L. Glazman, J.G.E. Harris, Persistent currents in normal metal rings, Science 326 (2009) 272–275.
[36] H. Bluhm, N.C. Koshnick, J.A. Bert, M.E. Huber, K.A. Moler, Persistent currents in normal metal rings, Phys. Rev. Lett. 102 (2009) 136802.
[37] M.A. Castellanos-Beltran, D.Q. Ngo, W.E. Shanks, A.B. Jayich, J.G.E. Harris, Measurement of the full distribution of persistent current in normal-metal rings, Phys. Rev. Lett. 110 (2013) 156801.
[38] H.-F. Cheung, Y. Gefen, E.K. Riedel, W.-H. Shih, Persistent currents in small one-dimensional metal rings, Phys. Rev. B 37 (1988) 6050–6062.
[39] F. von Oppen, E.K. Riedel, Average persistent current in a mesoscopic ring, Phys. Rev. Lett. 66 (1991) 84–87.
[40] J.F. Weisz, R. Kishore, F.V. Kusmartsev, Persistent current in isolated mesoscopic rings, Phys. Rev. B 49 (1994) 8126–8131.
[41] T. Chakraborty, P. Pietiläinen, Persistent currents in a quantum ring: effects of impurities and interactions, Phys. Rev. B 52 (1995) 1932–1935.
[42] Y.V. Pershin, C. Piermarocchi, Persistent and radiation-induced currents in distorted quantum rings, Phys. Rev. B 72 (2005) 125348.
[43] A. Bruno-Alfonso, A. Latgé, Quantum rings of arbitrary shape and non-uniform width in a threading magnetic field, Phys. Rev. B 77 (2008) 205303.
[44] H. Bary-Soroker, O. Entin-Wohlman, Y. Imry, Persistent currents of noninteracting electrons in one-, two-, and three-dimensional thin rings, Phys. Rev. B 82 (2010) 144202.
[45] L. Ying, Y.-C. Lai, Robustness of persistent currents in two-dimensional Dirac systems with disorder, Phys. Rev. B 96 (2017) 165407.
[46] H.-Y. Xu, L. Huang, Y.-C. Lai, C. Grebogi, Superpersistent currents and whispering gallery modes in relativistic quantum chaotic systems, Sci. Rep. 5 (2015) 8963.
[47] H. Xu, L. Huang, Y.-C. Lai, A robust relativistic quantum two-level system with edge-dependent currents and spin polarization, Europhys. Lett. 115 (2016) 20005.
[48] A.H.C. Neto, F. Guinea, N.M.R. Peres, Edge and surface states in the quantum Hall effect in graphene, Phys. Rev. B 73 (2006) 205408.
[49] D.S.L. Abergel, V.M. Apalkov, T. Chakraborty, Interplay between valley polarization and electron-electron interaction in a graphene ring, Phys. Rev. B 78 (2008) 193405.
[50] C.W.J. Beenakker, A.R. Akhmerov, P. Recher, J. Tworzydło, Correspondence between Andreev reflection and Klein tunneling in bipolar graphene, Phys. Rev. B 77 (2008), 075409.
[51] M. Zarenia, J.M. Pereira, F.M. Peeters, G.A. Farias, Electrostatically confined quantum rings in bilayer graphene, Nano Lett. 9 (12) (2009) 4088–4092.
[52] R. Jackiw, A.I. Milstein, S.-Y. Pi, I.S. Terekhov, Induced current and Aharonov-Bohm effect in graphene, Phys. Rev. B 80 (2009), 033413.
[53] M.M. Ma, J.W. Ding, N. Xu, Odd-even width effect on persistent current in zigzag hexagonal graphene rings, Nanoscale 1 (2009) 387–390.
[54] M. Zarenia, J.M. Pereira, A. Chaves, F.M. Peeters, G.A. Farias, Simplified model for the energy levels of quantum rings in single layer and bilayer graphene, Phys. Rev. B 81 (2010), 045431.
[55] D. Soriano, J. Fernández-Rossier, Spontaneous persistent currents in a quantum spin Hall insulator, Phys. Rev. B 82 (2010) 161302.
[56] P. Michetti, P. Recher, Bound states and persistent currents in topological insulator rings, Phys. Rev. B 83 (2011) 125420.
[57] B.-L. Huang, M.-C. Chang, C.-Y. Mou, Persistent currents in a graphene ring with armchair edges, J. Phys. Condens. Matter 24 (2012) 245304.
[58] D. Faria, A. Latgé, S.E. Ulloa, N. Sandler, Currents and pseudomagnetic fields in strained graphene rings, Phys. Rev. B 87 (2013) 241403.
[59] D. Sticlet, B. Dóra, J. Cayssol, Persistent currents in Dirac fermion rings, Phys. Rev. B 88 (2013) 205401.
[60] N. Bolívar, E. Medina, B. Berche, Persistent charge and spin currents in the long-wavelength regime for graphene rings, Phys. Rev. B 89 (2014) 125413.
[61] A. Larkin, Y.N. Ovchinnikov, Quasiclassical method in the theory of superconductivity, Sov. Phys. JETP 28 (6) (1969) 1200–1205.
[62] C. von Keyserlingk, T. Rakovszky, F. Pollmann, S. Sondhi, Operator hydrodynamics, otocs, and entanglement growth in systems without conservation laws, Phys. Rev. X 8 (2) (2018), 021013.
[63] A. Nahum, S. Vijay, J. Haah, Operator spreading in random unitary circuits, Phys. Rev. X 8 (2) (2018), 021014.
[64] P. Hosur, X.-L. Qi, D.A. Roberts, B. Yoshida, Chaos in quantum channels, J. High Energy Phys. 2016 (2) (2016) 4.
[65] A. Nahum, J. Ruhman, S. Vijay, J. Haah, Quantum entanglement growth under random unitary dynamics, Phys. Rev. X 7 (3) (2017), 031016.
[66] J. Li, R. Fan, H. Wang, B. Ye, B. Zeng, H. Zhai, X. Peng, J. Du, Measuring out-of-time-order correlators on a nuclear magnetic resonance quantum simulator, Phys. Rev. X 7 (3) (2017), 031011.
[67] I. Kukuljan, S. Grozdanov, T. Prosen, Weak quantum chaos, Phys. Rev. B 96 (6) (2017), 060301.
[68] C.-J. Lin, O.I. Motrunich, Out-of-time-ordered correlators in a quantum ising chain, Phys. Rev. B 97 (14) (2018) 144304.
[69] K. Jensen, Chaos in ads 2 holography, Phys. Rev. Lett. 117 (11) (2016) 111601.
[70] A.M. García-García, B. Loureiro, A. Romero-Bermúdez, M. Tezuka, Chaotic-integrable transition in the sachdev-ye-kitaev model, Phys. Rev. Lett. 120 (24) (2018) 241603.
[71] D.A. Roberts, D. Stanford, Diagnosing chaos using four-point functions in two-dimensional conformal field theory, Phys. Rev. Lett. 115 (13) (2015) 131603.
[72] J. Maldacena, S.H. Shenker, D. Stanford, A bound on chaos, J. High Energy Phys. 2016 (8) (2016) 106.
[73] K. Hashimoto, K. Murata, K. Yoshida, Chaos in chiral condensates in gauge theories, Phys. Rev. Lett. 117 (23) (2016) 231602.
[74] K. Hashimoto, K. Murata, R. Yoshii, Out-of-time-order correlators in quantum mechanics, J. High Energy Phys. 2017 (10) (2017) 138.
[75] B. Dóra, M.A. Werner, C.P. Moca, Information scrambling at an impurity quantum critical point, Phys. Rev. B 96 (15) (2017) 155116.
[76] E.B. Rozenbaum, S. Ganeshan, V. Galitski, Lyapunov exponent and out-of-time-ordered correlator's growth rate in a chaotic system, Phys. Rev. Lett. 118 (2017), 086801.
[77] T. Hogg, B.A. Huberman, Recurrence phenomena in quantum dynamics, Phys. Rev. Lett. 48 (1982) 711–714.
[78] P. Strange, Relativistic quantum revivals, Phys. Rev. Lett. 104 (2010) 120403.
[79] M.A. Sepúlveda, S. Tomsovic, E.J. Heller, Semiclassical propagation: how long can it last? Phys. Rev. Lett. 69 (1992) 402–405.
[80] S. Tomsovic, J.H. Lefebvre, Can wave packet revivals occur in chaotic quantum systems? Phys. Rev. Lett. 79 (1997) 3629–3632.
[81] M.V. Berry, Quantum scars of classical closed orbits in phase-space, Proc. R. Soc. London Series A Math. Phys. Eng. Sci. 423 (1864) (1989) 219–231.
[82] H.A. Cerdeira, K. Furuya, B.A. Huberman, Lyapunov exponent for quantum dissipative systems, Phys. Rev. Lett. 61 (1988) 2511–2513.
[83] F. Haake, H. Wiedemann, K. Zyczkowski, Lapunov exponent for quantum mechanics, Ann. Phys. 1 (1992) 531–539.
[84] R. Blümel, Exponential sensitivity and chaos in quantum systems, Phys. Rev. Lett. 73 (1994) 428–431.
[85] R. Schack, Comment on "exponential sensitivity and chaos in quantum systems", Phys. Rev. Lett. 75 (1995), 581–581.
[86] R. Blümel, Blümel replies: Phys. Rev. Lett. 75 (1995), 582–582.
[87] I.L. Aleiner, A.I. Larkin, Divergence of classical trajectories and weak localization, Phys. Rev. B 54 (1996) 14423–14444.
[88] I.L. Aleiner, A.I. Larkin, Role of divergence of classical trajectories in quantum chaos, Phys. Rev. E 55 (1997) R1243–R1246.
[89] O. Agam, I. Aleiner, A. Larkin, Shot noise in chaotic systems: "classical" to quantum crossover, Phys. Rev. Lett. 85 (2000) 3153–3156.
[90] J. Robbins, M. Berry, Discordance between quantum and classical correlation moments for chaotic systems, J. Phys. A 25 (15) (1992) L961.
[91] Y. Gu, X.-L. Qi, Fractional statistics and the butterfly effect, J. High Energy Phys. 2016 (8) (2016) 129.
[92] M. Robnik, Quantising a generic family of billiards with analytic boundaries, J. Phys. A 17 (5) (1984) 1049.
[93] H. Xu, L. Huang, Y.-C. Lai, C. Grebogi, Chiral scars in chaotic Dirac fermion systems, Phys. Rev. Lett. 110 (6) (2013), 064102.
[94] J.D. Bjorken, S.D. Drell, Relativistic Quantum Mechanics, McGraw-Hill, New York, 1964.

[95] T. García, N.A. Cordero, E. Romera, Zitterbewegung and quantum revivals in monolayer graphene quantum dots in magnetic fields, Phys. Rev. B 89 (2014), 075416.
[96] D.A. Roberts, D. Stanford, L. Susskind, Localized shocks, J. High Energy Phys. 2015 (3) (2015) 51.
[97] I. García-Mata, M. Saraceno, R.A. Jalabert, A.J. Roncaglia, D.A. Wisniacki, Chaos signatures in the short and long time behavior of the out-of-time ordered correlator, Phys. Rev. Lett. 121 (21) (2018) 210601.
[98] R.W. Robinett, Quantum wave packet revivals, Phys. Rep. 392 (1–2) (2004), 1–119.
[99] R. Robinett, S. Heppelmann, Quantum wave-packet revivals in circular billiards, Phys. Rev. A 65 (6) (2002), 062103.
[100] A. Relano, J. Gómez, R. Molina, J. Retamosa, E. Faleiro, Quantum chaos and 1/f noise, Phys. Rev. Lett. 89 (24) (2002) 244102.
[101] E. Faleiro, J. Gómez, R. Molina, L. Munoz, A. Relano, J. Retamosa, Theoretical derivation of 1/f noise in quantum chaos, Phys. Rev. Lett. 93 (24) (2004) 244101.
[102] J. Gómez, A. Relaño, J. Retamosa, E. Faleiro, L. Salasnich, M. Vraničar, M. Robnik, 1/f α noise in spectral fluctuations of quantum systems, Phys. Rev. Lett. 94 (8) (2005), 084101.
[103] R.A. Jalabert, H.M. Pastawski, Environment-independent decoherence rate in classically chaotic systems, Phys. Rev. Lett. 86 (12) (2001) 2490.
[104] Q. Su, B. Smetanko, R. Grobe, Relativistic suppression of wave packet spreading, Opt. Express 2 (7) (1998) 277–281.
[105] D. Matrasulov, G. Milibaeva, U. Salomov, B. Sundaram, Relativistic kicked rotor, Phys. Rev. E 72 (1) (2005), 016213.
[106] M.L. Mehta, Random Matrices, Academic, Boston, 1991.
[107] T. Guhr, A. Müller-Groeling, H.A. Weidenmüller, Random-matrix theories in quantum physics: common concepts, Phys. Rep. 299 (4–6) (1998), 189–425.
[108] P. So, S.M. Anlage, E. Ott, R.N. Oerter, Wave chaos experiments with and without time reversal symmetry: gue and goe statistics, Phys. Rev. Lett. 74 (14) (1995) 2662.
[109] A. Rehemanjiang, M. Allgaier, C. Joyner, S. Müller, M. Sieber, U. Kuhl, H.-J. Stöckmann, Microwave realization of the Gaussian symplectic ensemble, Phys. Rev. Lett. 117 (6) (2016), 064101.
[110] L. Huang, Y.-C. Lai, C. Grebogi, Relativistic quantum level-spacing statistics in chaotic graphene billiards, Phys. Rev. E 81 (5) (2010), 055203.
[111] L. Huang, Y.-C. Lai, C. Grebogi, Characteristics of level-spacing statistics in chaotic graphene billiards, Chaos 21 (2011), 013102.
[112] P. Yu, Z.-Y. Li, H.-Y. Xu, L. Huang, B. Dietz, C. Grebogi, Y.-C. Lai, Gaussian orthogonal ensemble statistics in graphene billiards with the shape of classically integrable billiards, Phys. Rev. E 94 (2016), 062214.
[113] J.S. Cotler, G. Gur-Ari, M. Hanada, J. Polchinski, P. Saad, S.H. Shenker, D. Stanford, A. Streicher, M. Tezuka, Black holes and random matrices, J. High Energy Phys. 2017 (5) (2017) 118.
[114] H. Gharibyan, M. Hanada, S.H. Shenker, M. Tezuka, Onset of random matrix behavior in scrambling systems, J. High Energy Phys. 2018 (7) (2018) 124.
[115] E.B. Rozenbaum, S. Ganeshan, V. Galitski, Universal level statistics of the out-of-time-ordered operator. Phys. Rev. B 100, American Physical Society, 2019, 035112.
[116] H. Gharibyan, M. Hanada, B. Swingle, M. Tezuka, Quantum lyapunov spectrum, J. High Energy Phys. 2019 (4) (2019) 82.
[117] F.W. Olver, D.W. Lozier, R.F. Boisvert, C.W. Clark, NIST Handbook of Mathematical Functions, Cambridge university press, New York, NY, 2010.